

¹ Chapter 1

² Charge monitoring

³ *The ATLAS Diamond Beam Monitor*

⁴ Particle detectors in high energy physics experiments need to meet very stringent
⁵ specifications, depending on the functionality and their position in the experiment.
⁶ In particular, the detectors close to the collision point are subject to high levels of
⁷ radiation. Then, they need to operate with a high spatial and temporal segmentation
⁸ to be able to precisely measure trajectories of hundreds of particles in very short
⁹ time. In addition, they need to be highly efficient. In terms of the structure, their
¹⁰ active sensing material has to be thin so as not to cause the particles to scatter
¹¹ or get stopped, which would worsen the measurements. This also means that they
¹² have to have a low heat dissipation so that the cooling system dimensions can be
¹³ minimised. Finally, they need to be able to operate stably for several years without
¹⁴ an intervention, because they are buried deep under tonnes of material and electronics.

¹⁵ The material of choice for the inner detector layers in the HEP experiments is
¹⁶ silicon. It can withstand relatively high doses of radiation, it is highly efficient (of the
¹⁷ order of $\sim 99.9\%$) and relatively low cost due to using existing industrial processes
¹⁸ for its production. Its downside is that, with increasing irradiation levels, it needs to
¹⁹ be cooled to increasingly low temperatures to ensure a stable operation. This is not
²⁰ the case with diamond. In addition, diamond has a lower radiation damage factor,
²¹ which means it can operate in a radiation-heavy environment for a longer period.

²² The ATLAS Diamond Beam Monitor (DBM) [] is a novel high energy charged
²³ particle detector. Its function is to measure luminosity and beam background in the
²⁴ ATLAS experiment. Given its position in a region with a high radiation dose, di-
²⁵ amond was chosen as the sensing material. The monitor's pCVD diamond sensors
²⁶ are instrumented with pixellated FE-I4 front-end chips. The pCVD diamond sensor
²⁷ material was chosen to ensure the durability of the sensors in a radiation-hard envi-
²⁸ ronment and the size of its active area. The DBM is not the first diamond detector
²⁹ used in HEP, but it is the largest pixellated detector installed thus far, as shown in
³⁰ figure 1.1. It was designed as an upgrade to the existing luminosity monitor called the
³¹ Beam Conditions Monitor (BCM) [] consisting of eight diamond pad detectors, which

1.1. LUMINOSITY MEASUREMENTS

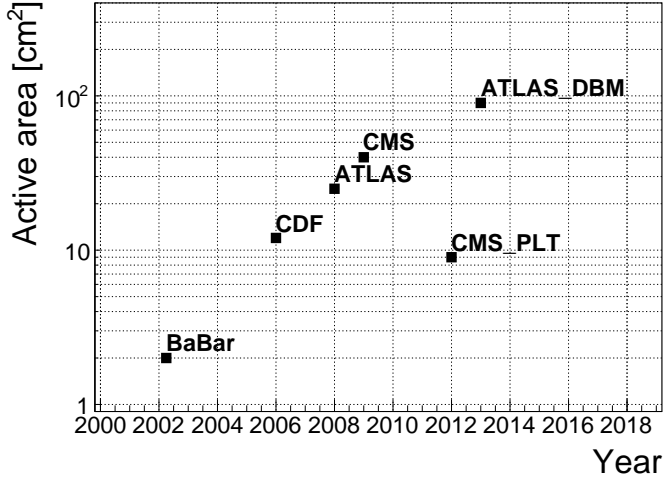


Figure 1.1: Diamond detectors installed in high-energy physics experiments in the last decade, sorted by the active sensor area. The first four detectors from the left are radiation monitors whereas the right two are pixel trackers.

is able to perform precise time-of-flight (ToF) measurements. The DBM complements the BCM’s features by implementing tracking capability. Its pixelated front-end electronics significantly increase the spatial resolution of the system. Furthermore, the DBM is able to distinguish particle tracks originating in the collision region from the background hits. This capability is a result of its projective geometry pointing towards the interaction region. This chapter first describes the principles of luminosity measurements. It then explains how the DBM carries out this task. Finally, some results from tests and from the real collisions are presented.

When a particle traverses a sensor plane, a hit is recorded in the corresponding pixel. Thus, a precise spatial and timing information of the hit is extracted. With three or more sensors stacked one behind the other, it is also possible to define the particle’s trajectory. This is the case with the DBM. Its projective geometry allows the particles to be tracked if they traverse the sensor planes. The DBM relates the luminosity to the number of particle tracks that originate from the collision region of the ATLAS experiment. Particles that hit the DBM from other directions are rejected as background radiation.

1.1 Luminosity measurements

Luminosity is one of the most important parameters of a particle collider. It is a measurement of the rate of particle collisions that are produced by two particle beams. It can be described as a function of beam parameters, such as: the number of colliding bunch pairs, the revolution frequency, the number of particles in each bunch and the transverse bunch dimensions. The first four parameters are well defined. However, the transverse bunch dimensions have to be determined experimentally

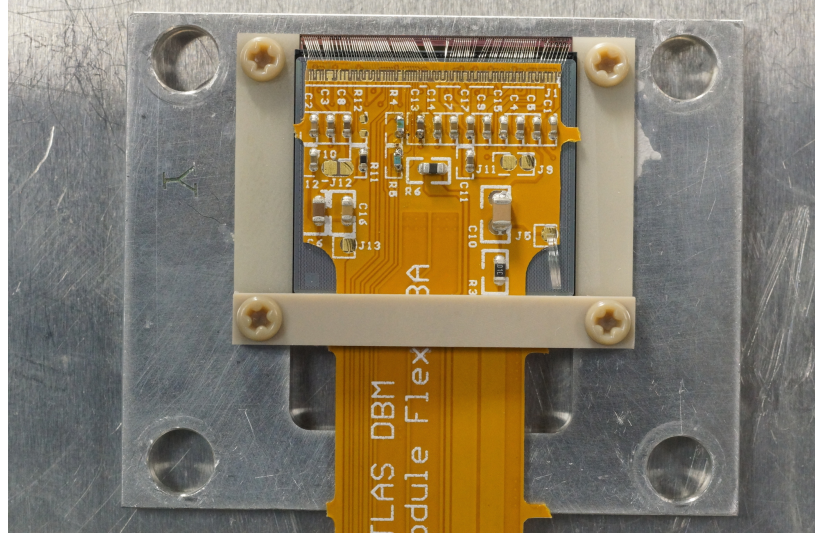


Figure 1.2: DBM module, top-down view. Visible is the flexible PCB with signal and power connections, the silicon sensor and a part of the FE-I4. Wire bonds from the PCB to the FE-I4 and to the sensor are also visible.

55 during calibration. The ATLAS experiment uses the *van der Meer scan* [1] during
56 low-luminosity runs to calibrate the luminosity detectors. This scan is performed
57 by displacing one beam in a given direction and measuring the rate of interactions
58 as a function of the displacement. Transverse charge density of the bunches can be
59 estimated on the basis of the interaction rate. The calibrated luminosity detectors
60 can then operate during high-luminosity runs.

61 One approach to luminosity monitoring is to count the number of particles pro-
62 duced by the collisions. The luminosity is then proportional to the number of detected
63 particles. A detector has to be capable of distinguishing individual particles that fly
64 from the interaction point through the active sensor area. If the detector has at least
65 three layers, it can reconstruct the particles' tracks, which in turn yields more infor-
66 mation on the their trajectory. This is one reason why detectors with a high timing-
67 and spatial segmentation are more suitable for these applications. The second reason
68 is that, with a high spatial segmentation, the detector does not saturate even at high
69 particle fluencies.

70 **1.2 Diamond pixel module**

71 The two most important parts of the diamond pixel module, which is shown in fig-
72 ure 1.2, are the sensor, which detects ionising radiation, and the pixellated front-end
73 chip, which collects the ionised charge with a high spatial segmentation, processes the
74 recorded data and sends them to the readout system. This section describes these
75 two main parts of the module and their interconnection.

1.2. DIAMOND PIXEL MODULE



Figure 1.3: A pCVD wafer. The golden dots on the surface are the electrodes that are applied during the qualification test. The wafer is measured across the surface to find the regions with the highest efficiency.

76 1.2.1 Sensors

77 The DBM modules are instrumented with two types of sensors – pCVD diamond and
78 silicon. The silicon sensors are used as a fallback solution because there were simply
79 not enough high-quality diamond sensors available. In addition, a comparative study
80 of irradiation damage between silicon and diamond can be made with such a hybrid
81 system.

82 **Diamond sensors** The target material for this application is pVCD diamond. The
83 reason for this is that the active area of an individual sensor must be approximately
84 4 cm^2 , which is too large for the sCVD diamond. pCVD material is also a bit
85 cheaper, which makes a detector with a large active area more feasible to build. The
86 material is provided by three companies: DDL, E6 and II-IV and it is grown in
87 15 cm wafers, as seen in figure 1.3. The target thickness of the wafers is 500 μm and
88 the minimum required charge collection efficiency is 40 % ($\text{CCD} \geq 200 \mu\text{m}$). They
89 need to be operated at bias voltages between 600–1000 V. On one side there is a
90 single gold electrode applied across the entire surface. On the other side a pixellated
91 metallisation is added.

92 **Silicon sensors** are standard $n^+ - in - n$ planar sensors with a 200 μm thickness
93 and were mostly fabricated at CiS [], a company from Ertfurt, Germany. They are
94 designed to have nearly a 100 % efficiency when non-irradiated. Their bulk resistivity
95 is between 2–5 $\text{k}\Omega\text{cm}$ and they were diffusion oxygenated at 1150 °C for 24 hours to

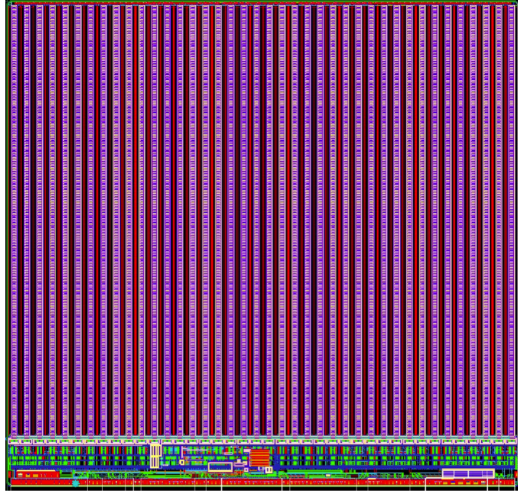


Figure 1.4: FE-I4 layout, top-down view. The pink area are pixels grouped into columns, the green area below is the common logic and the red strip at the bottom are the wire bond pads.

increase their radiation hardness. One side is segmented into pixels. Guard rings at the edges of the sensor provide a controlled drop in potential, reducing the possibility of shorts at maximum design bias voltages of the order of 1000 V.

1.2.2 Front-end electronics

The FE-I4 (front-end version four) [1] is an ASIC pixel chip designed specifically for the ATLAS pixel detector upgrade. It is built as a successor to the current pixel chip FE-I3, surpassing it in size of the active area ($4\times$ larger) as well as the number of channels/pixels ($10\times$ more). 336 such FE-I4 modules are used in the newly installed pixel layer called the Insertable B-Layer (IBL) [2]. The DBM is also instrumented with these chips. The FE-I4's integrated circuit contains readout circuitry for 26880 pixels arranged in 80 columns on a $250\text{ }\mu\text{m}$ pitch and 336 rows on a $50\text{ }\mu\text{m}$ pitch. The size of the active area is therefore $20.0\times16.8\text{ mm}^2$. This fine granularity allows for a high-precision particle tracking. The chip operates at 40 MHz with a 25 ns acquisition window, which corresponds to the spacing of the particle bunches in the LHC. It is hence able to correlate hits/tracks to their corresponding bunch. Furthermore, each pixel is capable of measuring the deposited charge of a detected particle by using the Time-over-Threshold (ToT) method. Finally, the FEI4 has been designed to withstand a radiation dose up to 300 MGy. This ensures a longterm stability in the radiation hard forward region of the ATLAS experiment.

Each pixel is designed as a separate entity. Its electrical chain is shown in figure 1.5. The bump-bond pad – the connection to the outside of the chip – is the input of the electrical chain, connected to a free-running amplification stage with adjustable shaping using a 4-bit register at the feedback branch. The analog amplifier is designed to collect negative charge, therefore electrons. The output is routed through

1.2. DIAMOND PIXEL MODULE

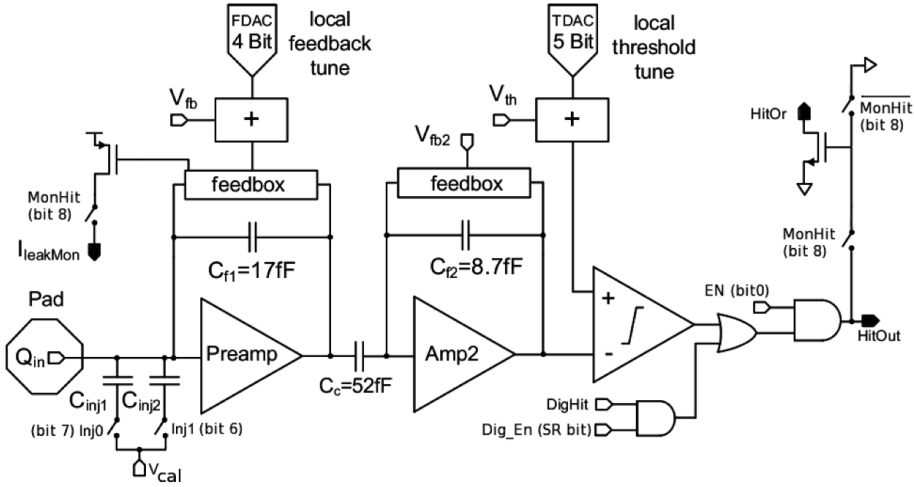


Figure 1.5: Schematic of an analog pixel. Courtesy of the FE-I4 collaboration.

120 a discriminator with an adjustable threshold. This value in effect defines the level
 121 at which the circuit detects a hit. In addition, there is a counter of the clock cycles
 122 (25 ns sampling) during which the signal is above the discriminator threshold. The
 123 value of the counter is proportional to the collected charge. The logic gates at the end
 124 of the chain are used to enable/disable the pixel and to issue a so-called HitOr flag –
 125 this signal is set whenever at least one of the pixels was hit and is used as a trigger
 126 for the readout. The output of the chain – HitOut – is routed into the logic of the
 127 chip where it is buffered and eventually sent out to the readout system. The module
 128 receives all its commands from the system via a 40 MHz LVDS line. The commands
 129 are either settings for the pixel registers or triggers that start the data readout. The
 130 data are sent via an LVDS line at up to 320 Mbit/s, but by default at 160 Mbit/s,
 131 four times faster than the clock of the device. This allows the chip to clear out its
 132 buffers before new data are recorded, thus avoiding dead time and data pile-up. The
 133 FE-I4 has been successfully tested for trigger rates of up to 300 kHz.

134 The DBM uses pCVD diamond with $d_C = 500 \mu\text{m}$ thickness and silicon with
 135 $d_{Si} = 200 \mu\text{m}$ thickness as a sensor material. The resulting most probable value
 136 (MPV) of the deposited charge for a minimum ionising particle (MIP) is calculated
 137 with the formula $Q_s = d \cdot E_{e-h}$ and equals 18000 electrons and 17800 electrons,
 138 respectively, at a full charge collection efficiency. Unfortunately this is not the case
 139 with the pCVD material, whereby the expected charge collection efficiency is of the
 140 order of 50 % – around 9000 e. This value further decreases with received irradiation
 141 dose. Therefore in order to detect the particles depositing energy on the far left side
 142 of the landau spectrum, the threshold has to be set to a significantly lower value.
 143 On the other hand, if the threshold set too low, it also detects the electronic noise
 144 and stores a false noisy hit. With the typical noise amplitudes being in the range of
 145 120–200 e, a safe threshold range would be between $Th = 1000\text{--}3000$ e. The target
 146 for the DBM is to lower the threshold down to 800 e.

The analog amplifier is implemented in two stages to get a fast rise time at a low noise and a low power consumption. The output signal of the analog amplifier has a triangular shape with a fast rise time and a long decay. The shape can be adjusted by tuning the amplifier feedback loop. Its length is proportional to the collected charge, but it needs to be calibrated first. This is done by means of two injection capacitors, $C_{\text{inj}1}$ and $C_{\text{inj}2}$, seen in figure 1.5 with well defined capacitances. First, the charge $Q_{\text{cal}} = V_{\text{cal}} \cdot (C_{\text{inj}1} + C_{\text{inj}2})$ is injected into the analog chain. Then the length of the output pulse is measured and finally the feedback value is changed to either lengthen or shorten the pulse in order to get to the required duration t_{cal} . The typical values are $Q_{\text{cal}} = 5000 - 16000$ e at the time $t_{\text{cal}} = 5 - 10$ ToT. The target values depend on the sensor, the type of a radioactive source and the application. Therefore the initial threshold Th at 1 ToT and the calibrated value Q_{cal} at t_{cal} ToT give us a linear scale of collected charge with respect to time over threshold. However, in practice this relation is nonlinear for lower thresholds, but since the goal of the measurements is to track the particles rather than to measure their deposited energy precisely, this is sufficient.

1.3 Module assembly and quality control

Parts for the detector arrived separately and were assembled into modules at CERN’s DSF lab after being checked for production faults. The assembled modules underwent a series of quality control (QC) and burn-in tests to determine their quality, efficiency and long-term stability.

1.3.1 Assembly

A single-chip module consists of a pixel module, a flexible PCB and the supporting mechanics (a ceramic plate and an aluminium plate). The chip arrives already bump-bonded to the sensor, be it diamond or silicon. First it is glued to the ceramic plate on one side and to the PCB on the other using either Araldite 2011 or Staystik 672/472. The choice of glue was a topic of a lengthy discussion. Staystik is re-workable and has a very high thermal conductivity. The latter is important because the FE-I4 chips tend to heat up significantly and need a good heat sink. The problem is that it has a curing temperature of 160/170 °C. This temperature may cause some unwanted stress build-up between the FE-I4 and the diamond sensor due to different coefficients of thermal expansion, pulling them apart. This would disconnect the pixels, yielding large regions of the module insensitive to radiation. To avoid this, an alternative glue was tried. Araldite 2011 can be cured at lower temperatures – down to RT – but it has a lower heat conductivity. In the end Araldite is used as the safer option. However, due to the longer curing, the entire assembly process using Araldite is extended to two working days. After curing, the module is wire-bonded and attached to the aluminium plate using screws made up of a radiation-resistant PEEK plastic. They have to be tightened with a great care, because their screw head is only 0.2–0.6 mm

1.3. MODULE ASSEMBLY AND QUALITY CONTROL

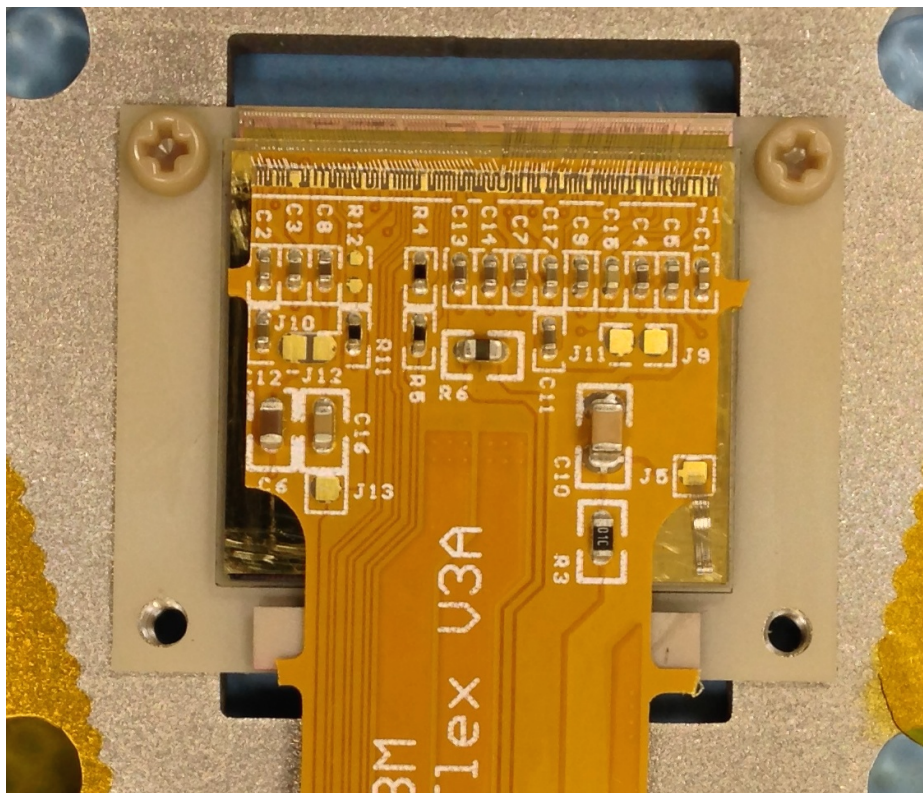


Figure 1.6: An assembled DBM module.

186 away from the sensor edge – the sensor displacement tolerance during gluing is of the
187 order of 0.5 mm. Finally, the module is put in an aluminium carrier which protects
188 it from mechanical damage or electrostatic discharges. Figure ?? shows an assembled
189 module.

190 1.3.2 Testing

191 The modules are tested in the lab using an RCE readout system and a moving stage
192 with two degrees of freedom. They are placed onto the stage and connected to the
193 readout system and the power supplies. After ensuring the low- and high voltage
194 connectivity they are checked for the signal connectivity. If everything is operational,
195 a series of automated tests is run. Each of these tests calibrates a certain value within
196 a pixel, whether it is the signal threshold or the value for integrated charge. These
197 are tuned in a way that the response to a predefined calibration signal is uniform for
198 all pixels across the sensor. This procedure is referred to as *tuning*.

199 When the modules are tuned, they are tested using a ^{90}Sr radioactive source. Two
200 things are checked: 1) operation of all pixels and 2) sensor efficiency. The first test
201 is carried out by moving the module slowly under the source while taking data so
202 that the entire surface is scanned uniformly. The resulting occupancy map reveals
203 any pixels that are not electrically coupled to the sensor via bump bonds. This is an
204 important step in the DBM QC procedure, because it turned out that a significant

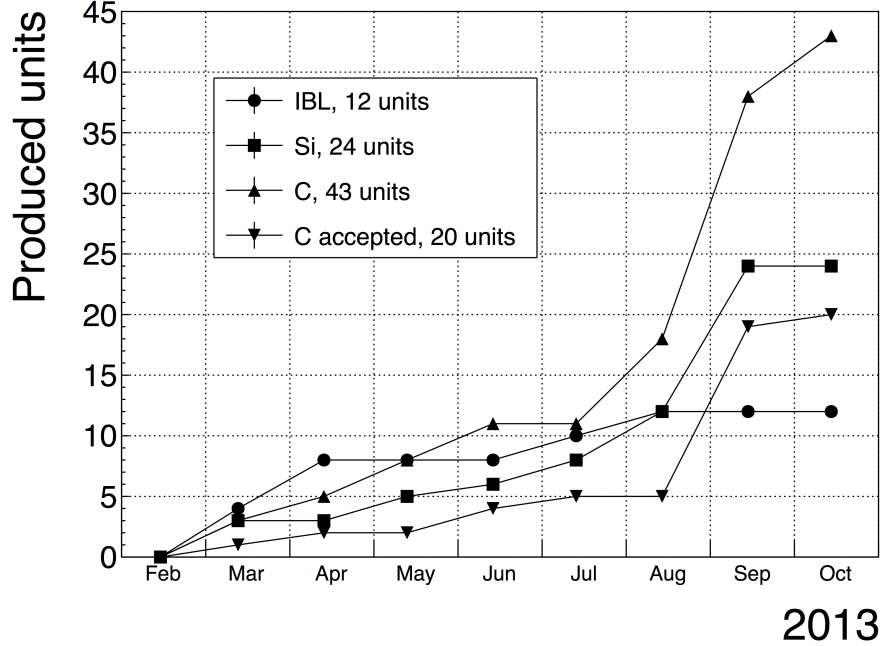


Figure 1.7: Module production with time.

portion of the flip-chipped diamond sensors exhibited very poor connectivity. The disconnected regions on the faulty modules ranged anywhere from 0.5–80 % of the overall active surface. In two cases the sensor was even completely detached from the chip. Therefore the pixel connectivity turns out to be the most important qualification factor in the QC procedure. Unfortunately the only way to check it at the moment is to fully assemble a module and test it using a radioactive source. If the module turns out to be of poor quality, it is disassembled and sent for rework. The turnover time of this operation is of the order of one month, which affected the DBM installation schedule significantly.

Only the modules that passed the pixel connectivity test undergo the second test stage in which the sensor’s efficiency was estimated. A scintillator is placed underneath the module and is used as a trigger. A particle that crosses the DBM module and hits the scintillator, triggers the module readout. In the end, the number of triggers is compared to the number of hits/clusters recorded by the module. The resulting ratio gives an estimate of the sensor’s detection efficiency. The real sensor efficiency can only be measured in a particle beam and using a beam telescope as a reference detector. Nonetheless, the *pseudo-efficiency* gives a rough estimate of the sensor’s quality.

The results for the DBM QC are shown in section 1.4. All in all, 79 modules went through the QC procedure – 43 diamond modules and 36 silicon modules, 12 of the latter only for testing purposes. Figure 1.7 shows their production with time. 18 diamond modules and 6 silicon modules were in the end chosen to be made up into DBM telescopes and installed into ATLAS.

1.3. MODULE ASSEMBLY AND QUALITY CONTROL

228 A very important issue is the so called erratic current. This term describes the
229 leakage current in a pCVD diamond that becomes unstable. It can develop gradually
230 or can be triggered with a β source. Spikes appear in the otherwise stable leakage
231 current. They can be up to three orders of magnitude higher than the base current.
232 Sometimes the current also suddenly increases for a few orders of magnitude and stays
233 at that level (e.g. from the initial 1 nA to 3 μ A). The amplitude differs in magnitude
234 from sensor to sensor. This effect is still not fully explained, but the hypothesis
235 is that the charges find a conductive channel along the grain boundaries, causing
236 discharges. These discharges are picked up by the pixel amplifiers in the FE-I4. A
237 single discharge can trigger a group of up to \sim 500 pixels, resulting in a *blob* on the
238 detector occupancy map. Sometimes the conductive channel stays in a conductive
239 state, making one or more pixels always to fire. These pixels only use the bandwidth
240 of the readout channel, so they have to be masked out during measurements.

241 1.3.3 Installation and commissioning

242 The DBM modules that passed the QC tests were assembled into telescopes – sets of
243 three modules one behind the other with a spacing of 50 mm. Of the 18 diamond and
244 6 silicon modules, 6 diamond and 2 silicon modules were built. A special care was
245 taken when choosing the sets of three diamonds. The modules with a similar pseudo-
246 efficiency, leakage current, maximum stable high voltage and shape of disconnected
247 regions were grouped together. After assembly into telescopes, the modules were
248 tested for their connectivity. Then the high voltage was applied and the leakage
249 current was observed. This was an important point to check because all three modules
250 shared the same high voltage channel. Any instabilities on one of the modules would
251 cause problems on the other two. This would for instance happen if one of the modules
252 had a much lower breakdown voltage.

253 Due to time constraints, the telescopes were not built at the same time but in-
254 stead the production was pipelined. As soon as two telescopes were ready, they were
255 transported to Point 1 – the site where parts of the ATLAS detector were being put
256 together. There they were prepared for installation onto the pixel detector struc-
257 ture that had been extracted from ATLAS due to pixel detector commissioning. The
258 commissioning was nearing completion, so the technicians were preparing the detec-
259 tor for re-insertion. The cylindrical structure was being closed off by four new service
260 quarter-panels (nSQPs). This meant that with every day the access to the place
261 of installation of the DBM was more difficult. The first two telescopes were still put
262 into place when only one nSQP was in place. This allowed the installation process
263 to be carried out from both sides. This proved to be helpful, because the process
264 was lengthy and had to be done with great precision. It involved tightening several
265 screws on both sides of the telescopes, adding thermal paste on the aluminium joints
266 and removing the protective covers, revealing the fragile wire bonds. At the same
267 time the surrounding electronics and cables had to be left untouched. The lessons
268 learnt with the first part of the installation were helpful when installing the other tele-

269 scopes. The last two were fitted onto the structure when three nSQPs were already
270 in place, leaving only a narrow opening for access. The entire procedure was carried
271 out blind. After every installation, the telescopes were tested again. First, the low
272 voltage connectivity was checked and a set of tests was run on the FE-I4 front-end
273 chips. An eye diagram was made to estimate the quality of the signal transmission.
274 Then a ^{90}Sr source was used to perform a source test on three modules at the same
275 time. Leakage current was observed during the source test. The final test included
276 running four telescopes (all on one side) at a time. All the tests were successful and
277 the DBM was signed off.

278 1.4 Performance results

279 This section gives an overview of the performance results of the DBM modules
280 achieved during the QC and the test beam campaign. The source tests were per-
281 formed to check for disconnected regions in the sensors and to measure the diamond's
282 pseudo-efficiency. Only the modules with minimal disconnected regions and maxi-
283 mum pseudo-efficiency were chosen for installation.

284 1.4.1 Source tests

285 All modules went through the same procedure when tested using a ^{90}Sr source – to
286 check for disconnected regions and to measure the pseudo-efficiency.

287 The setup consisted of a placeholder for the ^{90}Sr source, an X-Y moving stage
288 with a holder for the module and a scintillator with a photomultiplier placed below
289 the source and the module. The scintillator was used as a trigger – when it detected a
290 particle, it triggered the readout of the module. If the module was placed in between
291 the source and the scintillator, the particle had to traverse the module to hit the
292 scintillator. Therefore, in the case of a module with a 100 % efficiency the triggered
293 data read out by the module would need to contain at least one hit in the module. In
294 reality the β particles scatter around the setup and sometimes hit the scintillator from
295 other directions, without incident the module. This produces empty triggers. The
296 phenomenon sets the limitation of measuring with a radioactive source as compared
297 to the measurements in a test beam, in which the particles in principle always travel
298 in one direction and their scattering is minimal.

299 The test for disconnected regions was carried out by moving the module under the
300 source in X and Y direction so that the exposure over the entire plane was uniform.
301 This resulted in an occupancy scan seen in figures 1.8a and 1.8b. The silicon module
302 had a very uniform occupancy plot. So much so that the features of the overlaying
303 flexible PCB can be observed. The rectangular shadows are the passive components
304 whereas the lines are the traces in the PCB. Furthermore, a circular-shaped edge of
305 the PCB can be seen on the bottom right side of the plot. These darker areas are
306 such because fewer electrons can penetrate the material with a high density. In the
307 case of the diamond, the features of the PCB can be observed as well, but are much

1.4. PERFORMANCE RESULTS

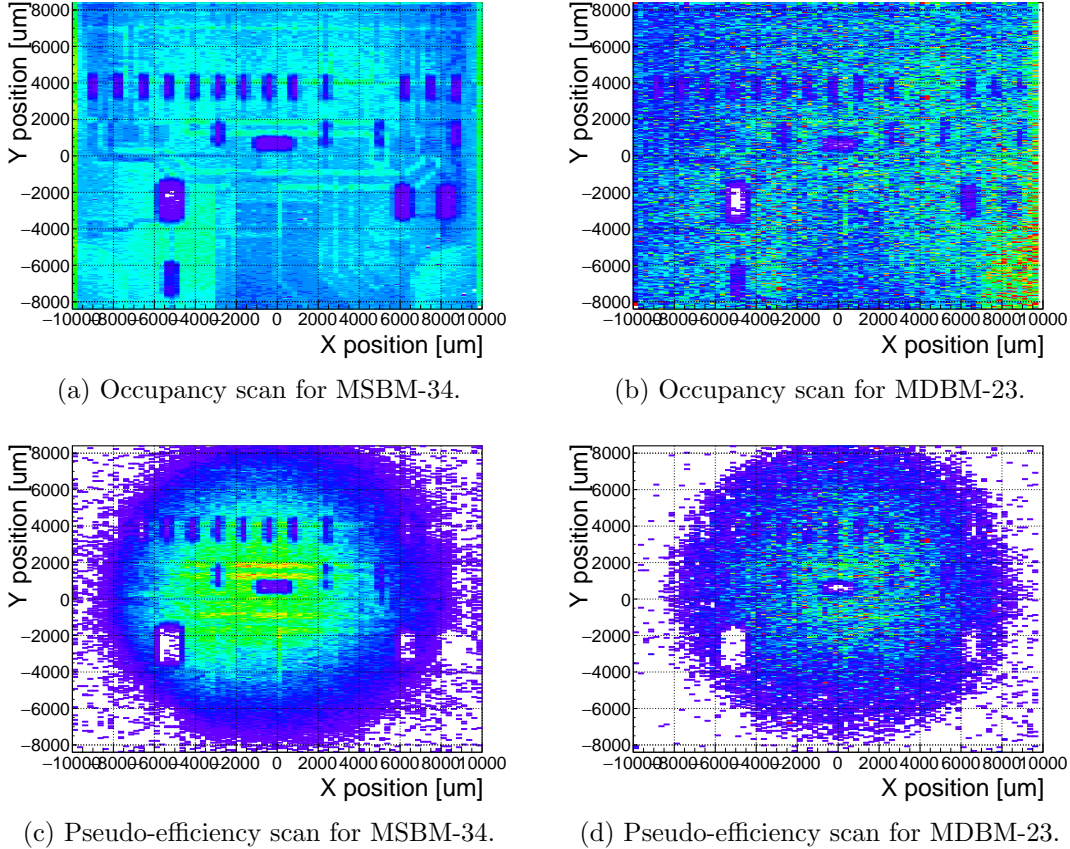
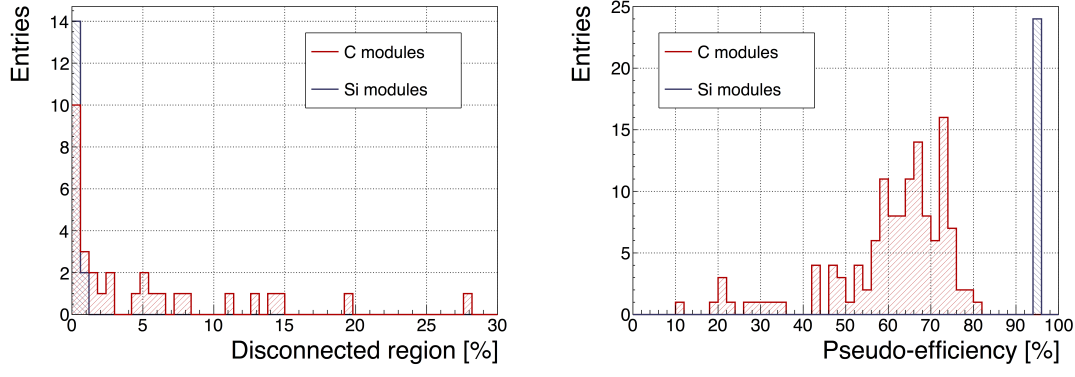


Figure 1.8: Occupancy and pseudo-efficiency scans for the silicon (left) and diamond sensor (right) to check for disconnected regions and estimate the sensor’s efficiency. Shadows of the electronic components are clearly visible because fewer electrons were able to traverse through such a higher amount of material.

308 less distinguishable. In principle, the plot is much more granulated – less uniform.
 309 This high variance in the diamond’s detection ability is due to the grain boundaries
 310 in the pCVD material which trap the drifting charges, rendering some regions much
 311 less efficient.

312 The pseudo-efficiency test was carried out by placing the module directly below the
 313 source and collimating the particles so that their trajectory was incident the module
 314 in the middle. For every trigger by the scintillator, a script checked whether there
 315 was a hit recorded in the module or not. The resulting ratio between the number
 316 of triggers and number of hits recorded in the module is a pseudo-efficiency – an
 317 estimation of the sensor’s efficiency. It cannot give a precise value due to the triggers
 318 produced by scattered particles, but at least gives a rough estimate.

319 Figure 1.9a shows the distribution of disconnected regions across all tested mod-
 320 ules. Silicon modules were performing as expected, with a minimum number of dis-
 321 connected pixels. The majority of the silicon modules yielded the pseudo-efficiency
 322 of $(94.3 \pm 0.2)\%$. Silicon sensors being 99.99 % efficient, this value was underesti-



(a) Disconnected regions for all modules derived from the occupancy scans. (b) Pseudo-efficiencies for all modules at various threshold and voltage settings.

Figure 1.9: Measurements of pseudo-efficiency and disconnected regions for all modules that went through the QC procedure.

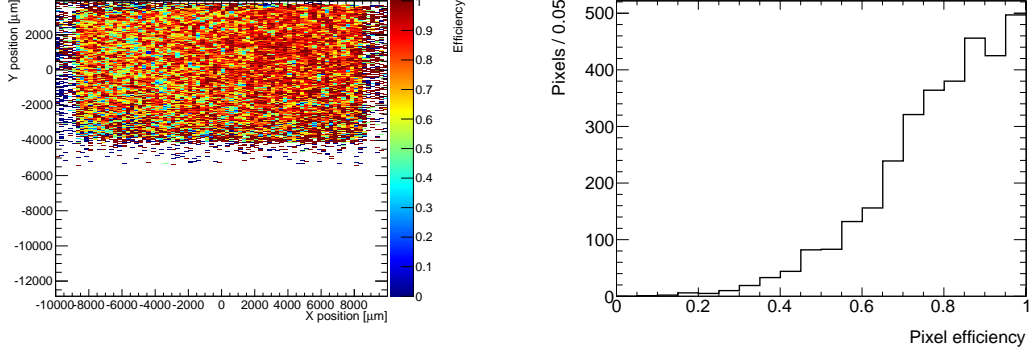
mated by about 5 %. The measured pseudo-efficiency of the diamond modules was (65 ± 7) %, with outliers down to 10 %. The value depended on the diamond quality, the set threshold and the applied bias voltage. The latter two settings were varied to check the behaviour of the modules under various conditions.

1.4.2 Test beam results

The first two assembled prototype DBM modules, MDBM-01 and MDBM-03, were tested at DESY, Hamburg, in a test beam facility. The aim of the measurements was to measure their efficiency, the spatial distribution of the efficiency and the effect of the beam on the disconnected regions. A silicon module MSBM-02 was measured to crosscheck the measurements. Since the silicon module is almost 100 % efficient, it was used as an “anchor” – the efficiency of the diamond module was measured relative to that of the silicon module. Two beam telescopes were used as reference systems: Kartel [], built by JSI institute from Ljubljana, and EUDET Aconite []. Both are instrumented with six Mimosa26 pixel planes and capable of tracking particles with a 2 μm pointing resolution.

The test beam prototypes did not meet the acceptance criteria for production DBM modules in the following areas: first, the stated CCDs were slightly below 200 μm , which would be the DBM minimum. Secondly, the applied bias voltages ranged from 1–2 V/ μm . In addition, the threshold cut could only be set to 1500 electrons, which is higher than the DBM minimum (1000 e). Nonetheless, the resulting module efficiencies were still in the range between 70–85 %.

To analyse the test beam data, Judith [] software framework was used. Judith is capable of synchronising data streams from several detector systems only connected via a trigger system, reconstructing tracks and calculating efficiency for the DUTs. It was also used to reconstruct and analyse the acquired Kartel test beam data together



(a) This is an efficiency distribution. Each bin corresponds to a single pixel. The triggering scintillator of the Kartel telescope was smaller than the DUT. Hence, the recorded hits can only be seen in the top half of the sensor.

(b) Pseudo-efficiencies for all modules at various threshold and voltage settings.

Figure 1.10: An efficiency study of a prototype DBM diamond module in a test beam. The statistics are low (~ 10 hits/pixel) as the data was collected during a short run.

³⁴⁸ with the silicon and diamond module as DUTs. A sample of the analysed data is
³⁴⁹ shown in figures 1.10a and 1.10b.

³⁵⁰ 1.5 Operation

³⁵¹ 1.5.1 Positioning

³⁵² The DBM is placed in the forward region of the ATLAS detector very close to the
³⁵³ beam pipe, as shown in figure 1.12. The mechanical structure that holds the sensor
³⁵⁴ planes is, due to its shape, referred to as a DBM telescope. A telescope is a system
³⁵⁵ that consists of several pixel sensors placed in series one behind the other. Each
³⁵⁶ DBM telescope houses three diamond pixel modules. Eight DBM telescopes reside
³⁵⁷ approximately 1 m away from the collision region, four on each side. They are tilted
³⁵⁸ with respect to the beam pipe for 10°. This is due to a specific phenomenon con-
³⁵⁹ nected to erratic (dark) currents in diamond. Studies have shown [] that the erratic
³⁶⁰ leakage currents that gradually develop in diamond can be suppressed under certain
³⁶¹ conditions. For instance, if a strong magnetic field is applied perpendicular to the
³⁶² electric field lines in the diamond bulk, the leakage current stabilises []. The DBM
³⁶³ was designed to exploit this phenomenon. The magnetic field lines in the ATLAS
³⁶⁴ experiment are parallel to the beam. Hence, an angular displacement of the sensor
³⁶⁵ with respect to the beam allows for the leakage current suppression. However, the
³⁶⁶ DBM telescopes still need to be directed towards the interaction region. Taking these
³⁶⁷ considerations into account, a 10° angle with respect to the beam pipe was chosen.
³⁶⁸ The influence of the magnetic field on the particle tracks at this angle is very low
³⁶⁹ as the field lines are almost parallel to the tracks. The tracks are therefore straight,



Figure 1.11: This photo highlights four telescopes installed onto the nSQPs and around the pipe.

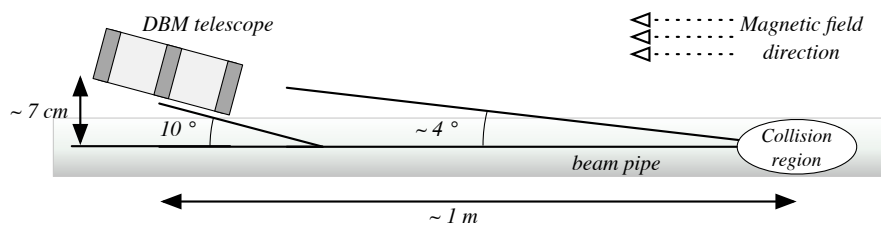


Figure 1.12: Position of the DBM in the ATLAS experiment.

³⁷⁰ which reduces the track reconstruction complexity.

³⁷¹ 1.5.2 Data taking during collisions

³⁷² The DBM has been commissioned in ATLAS and is now taking data. Several issues
³⁷³ still need to be resolved regarding the readout systems. Unfortunately, due to issues
³⁷⁴ with the low voltage power supply regulators, six out of 24 modules were damaged
³⁷⁵ during operation: four silicon and two diamond modules. The system configured
³⁷⁶ the modules into an unsteady state whereby they drew twice as much current as the
³⁷⁷ allowed maximum. This current most probably fused the wire bonds within minutes.

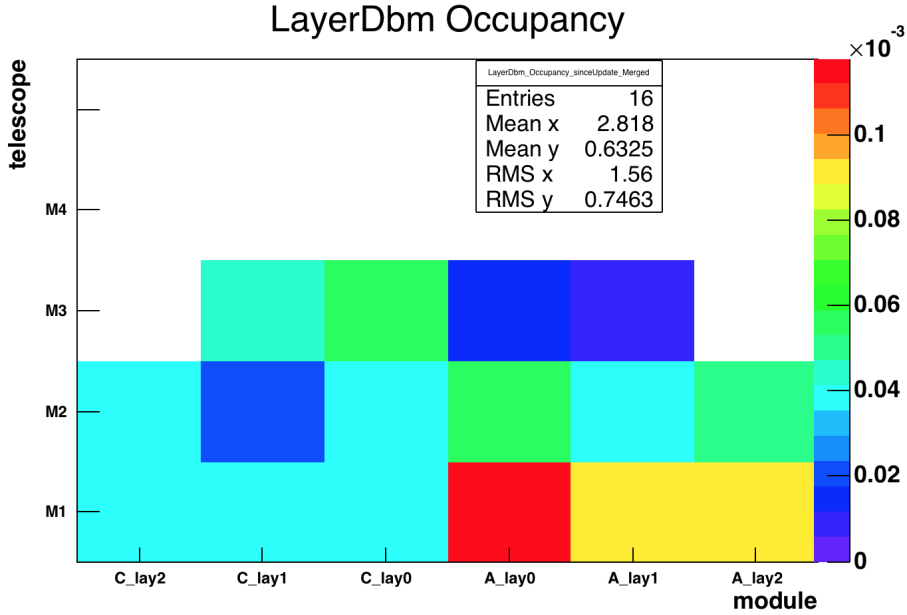


Figure 1.13: Occupancy of individual modules during collisions. Only 16 modules were taking data.

378 This has left only five diamond telescopes fully operational. The preliminary data
 379 obtained using the remaining telescopes show that the background rejection could
 380 indeed work.

381 The first step of the system test was to take data during collisions and check
 382 the occupancy in the individual modules. The occupancies were plotted side by side
 383 for comparison. Figure 1.13 shows some of the occupancy values. At the time, the
 384 readout system was not yet configured to read out all telescopes in parallel.

385 The second step was to test the detector's capability of particle tracking. Only one
 386 telescope was used to take data with the beam. If all three planes of the telescope
 387 were hit during a bunch crossing, a linear line was fitted to the hits. This line
 388 represented the particle's trajectory. It was projected towards the interaction point.
 389 Two parameters were calculated where the line is the closest to the interaction point:
 390 the radial distance and the longitudinal distance between the line and the interaction
 391 point, as shown in figure 1.14. This was done for the events with two colliding bunches
 392 as well as for events with only one, non-colliding bunch. The tracks recorded during
 393 the events with two colliding bunches could either come from the collisions or could
 394 be background scattering. Tracks recorded during a non-colliding bunch, on the
 395 other hand, are definitely background particles since, in principle, there should be no
 396 collisions taking place.

397 A comparison of the data acquired and depicted in figures 1.15a and 1.15b showed
 398 that, for the colliding bunches, the majority of the reconstructed tracks had the origin
 399 in the interaction point, with an expected spread in Z and R . For non-colliding
 400 bunches, the distribution is more spread out. In the Z_0 plot the distribution has one

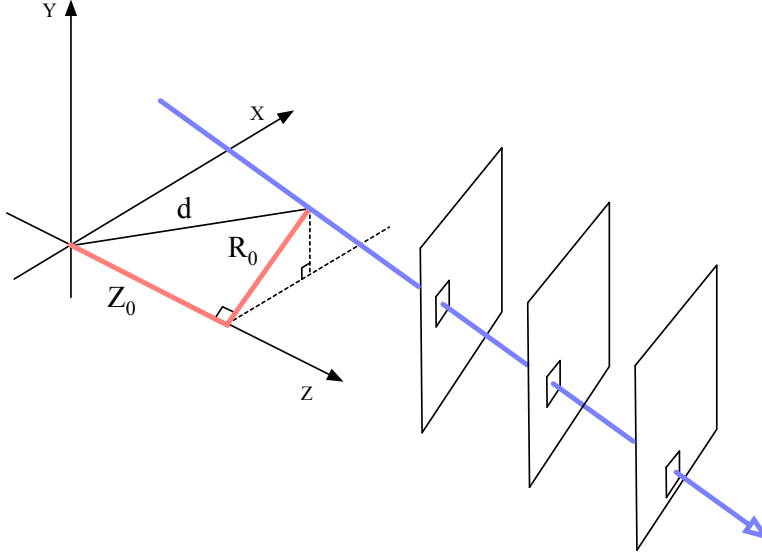


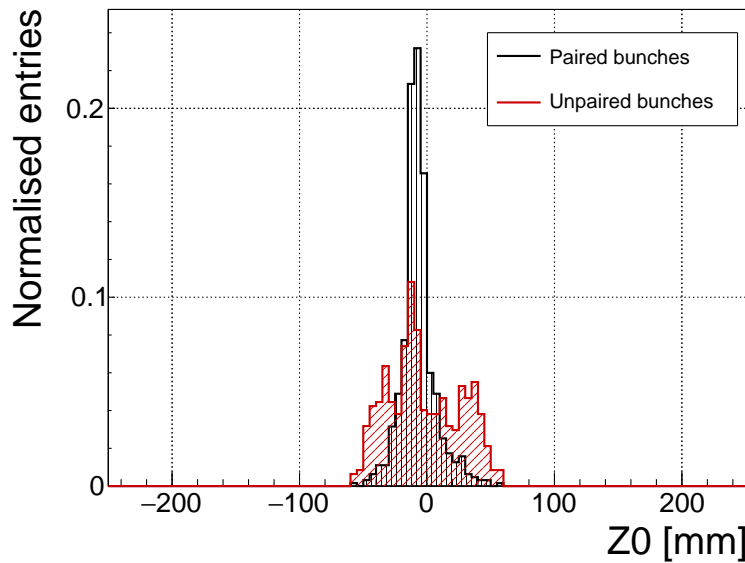
Figure 1.14: A diagram showing the radial distance R_0 and longitudinal distance Z_0 of the trajectory from the interaction point at the minimal distance d . Z is the axis along the beam line. Three module planes intercept a particle and reconstruct its trajectory.

⁴⁰¹ peak in the middle, which means that the empty RF buckets still held some particles.
⁴⁰² The two peaks on the sides, however, show that a significant number of tracks had
⁴⁰³ their origin at the radius of the beam pipe. Therefore these tracks were made by stray
⁴⁰⁴ protons colliding with the beam pipe. These collisions are unwanted as they do not
⁴⁰⁵ produce any meaningful physics while still damaging the ATLAS detector by means
⁴⁰⁶ of the scattered radiation.

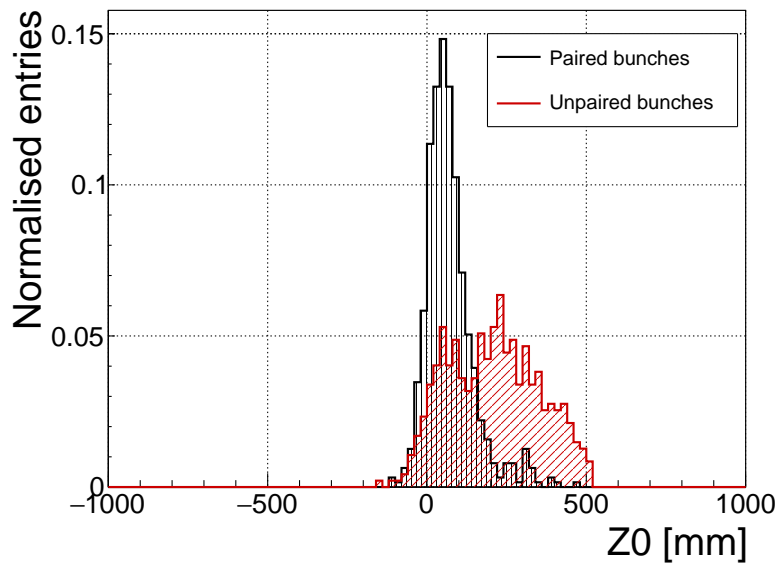
⁴⁰⁷ 1.6 Conclusion

⁴⁰⁸ The Diamond Beam Monitor has been designed as an upgrade to the existing lu-
⁴⁰⁹ minosity detectors in the ATLAS experiment. It is the first diamond pixel tracking
⁴¹⁰ detector installed in a high-energy physics experiment. The pixelated front-end elec-
⁴¹¹ tronic chips ensure precise spatial detection of the charged high-energy particles.
⁴¹² The projective geometry allows for particle tracking and background rejection. The
⁴¹³ detector is placed in a high-radiation forward region of the experiment. Therefore,
⁴¹⁴ radiation hardness of the chosen pCVD diamond sensors is an important requirement.
⁴¹⁵ The tests carried out in the test beam and in the laboratory confirmed that enough
⁴¹⁶ detector-grade DBM modules have been built to be installed in the experiment. The
⁴¹⁷ DBM is now running in ATLAS during collisions. Further improvements have to be
⁴¹⁸ made on the readout firmware before it is included in the main readout stream.

1.6. CONCLUSION



(a) Radial distance of the particle trajectories from the interaction point.



(b) Longitudinal distance of the particle trajectories (along the beam path) from the interaction point.

Figure 1.15: These two plots show two parameters of particle tracks recorded by one of the DBM telescopes: radial and longitudinal distance of the projected tracks from the interaction point.